Environmental Science Processes & Impacts

PAPER

View Article Online
View Journal

Cite this: DOI: 10.1039/c9em00341j

Atmosphere-terrestrial exchange of gaseous elemental mercury: parameterization improvement through direct comparison with measured ecosystem fluxes†

T. R. Khan, ‡*[a] D. Obrist, [b] Y. Agnan, [c] N. E. Selin [d] and J. A. Perlinger [a]

To simulate global mercury (Hg) dynamics in chemical transport models (CTMs), surface-atmosphere exchange of gaseous elemental mercury, Hg^0, is often parameterized based on resistance-based dry deposition schemes coupled with a re-emission function, mainly from soils. Despite extensive use of this approach, direct evaluations of this implementation against field observations of net Hg^0 exchange are lacking. In this study, we evaluate an existing net exchange parameterization (referred to here as the base model) by comparing modeled fluxes of Hg^0 to fluxes measured in the field using micrometeorological techniques. Comparisons were performed in two terrestrial ecosystems: a grassland site in Switzerland and an Arctic tundra site in Alaska, U.S., each including summer and winter seasons. The base model included the dry deposition and soil re-emission parameterizations from Zhang *et al.* (2003) and the global CTM GEOS-Chem, respectively. Comparisons of modeled and measured Hg^0 fluxes showed large discrepancies, particularly in the summer months when the base model overestimated daytime net deposition by approximately 9 and 2 ng m^{-2} h^{-1} at the grassland and tundra sites, respectively. In addition, the base model was unable to capture a measured nighttime net Hg^0 deposition and wintertime deposition. We conducted a series of sensitivity analyses and recommend that Hg simulations using CTMs: (i) reduce stomatal uptake of Hg^0 over grassland and tundra in models by a factor 5–7; (ii) increase nighttime net Hg^0 deposition, *e.g.*, by increasing ground and cuticular uptake by reducing the respective resistance terms by factors of 3–4 and 2–4, respectively; and (iii) implement a new soil re-emission parameterization to produce larger daytime emissions and lower nighttime emissions. We also compared leaf Hg^0 uptake over the growing season estimated by the dry deposition model against foliar Hg measurements, which revealed good agreement with the measured leaf Hg concentrations after adjusting the base model as suggested above. We conclude that the use of resistance-based models combined with the new soil re-emission flux parameterization is able to reproduce observed diel and seasonal patterns of Hg^0 exchange in these ecosystems. This approach can be used to improve model parameterizations for other ecosystems if flux measurements become available.

Received 16th July 2019
Accepted 12th September 2019

DOI: 10.1039/c9em00341j

rsc.li/espi

Environmental significance

In this study, we tested the performance of an existing surface-atmosphere exchange parameterization (base model) of elemental mercury (Hg^0) by comparing model results to whole-ecosystem net exchange fluxes measured at a grassland site in Switzerland and at an Arctic tundra site in Alaska, U.S. We found large discrepancies between base-modeled and measured exchange fluxes, particularly in the summer months when the base model substantially overestimated daytime net deposition at both sites. Another major shortcoming of the base model is its inability to capture a measured nighttime net Hg^0 deposition and wintertime deposition. Through a series of sensitivity tests, we demonstrate that an improved model *vs.* measurement agreement of exchange fluxes is achieved by (i) adjusting certain stomatal and non-stomatal resistance parameters in the base dry deposition model, and (ii) implementing a new soil re-emission model. To our knowledge, this is the first direct performance evaluation of Hg^0 net exchange parameterizations commonly used in chemical transport models with ecosystem level micrometeorological net exchange flux measurements. We conclude that the use of resistance-based deposition models combined with the new soil re-emission flux parameterization is able to reproduce observed diel and seasonal patterns of Hg^0 exchange in the two ecosystems. This approach can be used to improve Hg^0 exchange resistance model parameterizations for other ecosystem types, if flux data become available.

[a]*Department of Civil and Environmental Engineering, Michigan Technological University, Houghton, MI 49931, USA. E-mail: trkhan@mtu.edu*

[b]*Department of Environmental, Earth and Atmospheric Sciences, University of Massachusetts Lowell, Lowell, MA 01854, USA*

[c]*Earth and Life Institute, Université catholique de Louvain, 1348 Louvain-la-Neuve, Belgium*

[d]*Institute for Data, Systems, and Society, Department of Earth, Atmospheric, and Planetary Sciences, Massachusetts Institute of Technology, Cambridge, MA 02139, USA*

† Electronic supplementary information (ESI) available. See DOI: 10.1039/c9em00341j

‡ Current affiliation: Florida Solar Energy Center, a research institute of the University of Central Florida, Cocoa, FL 32922, USA.

1. Introduction

Atmosphere-surface exchange of gaseous elemental mercury (Hg^0) is an important component of the global atmospheric and terrestrial Hg budgets.[1–4] Despite advances in Hg^0 exchange flux measurements and their incorporation in chemical transport models (CTMs),[5] there remain large uncertainties with regard to the magnitudes and mechanistic understanding of bi-directional terrestrial surface-atmosphere exchange processes of Hg^0.[1,3] Hg^0 is the dominant form (approximately 95%) of Hg in the atmosphere and deposition of Hg^0 contributes a substantial fraction of total Hg deposition, particularly to vegetated ecosystems.[4,6] Evidence from stable Hg isotope studies suggests that atmospheric Hg^0 contributes 57–94% of total Hg to terrestrial ecosystems.[7–12] Moreover, geogenic emissions of Hg^0 contribute to atmospheric Hg,[13] and it is estimated that up to 65% of total present-day Hg emissions to the atmosphere could be attributed to secondary emission (re-emission) of Hg^0 from previous deposition residing in terrestrial and aquatic pools ("legacy emissions").[14,15] Given the importance of atmospheric Hg^0 as a source and sink to/from ecosystems and complex bi-directional exchange behavior,[16] an improved parameterization of atmosphere-surface exchange of Hg^0 in CTMs is necessary.

A resistance-based approach[17–20] is commonly used to model dry deposition of atmospheric constituents. For Hg^0, resistance-based deposition algorithms are implemented in all major global CTMs including TEAM,[21] GRAHM,[22] GEOS-Chem,[23,24] ECHMERIT,[25] GEM-MACH-Hg,[26] GLEMOS,[27] REMSAD[28] and CAM-Chem.[29] Similarly, regional models such as WRF-Chem[30] use a resistance-based approach for Hg^0 deposition. Only the regional CMAQ model contains a coupled bi-directional exchange parameterization (CMAQ-Hem and CCLM-CMAQ).[31] General uncertainties in modeling dry gaseous deposition using resistance-based algorithms include an inability to fully describe the physiological processes involved such as vegetation stomatal responses to environmental conditions,[32] lack of description of terrain complexity,[33] and exclusion of fast within-canopy chemical reactions.[19] For example, in an inter-comparison study of four resistance-based deposition models for reactive nitrogen species, Flechard *et al.*[34] reported factors of 2 to 3 disagreement between the models. Also, in a recent inter-comparison study of five dry gaseous deposition algorithms by Wu *et al.*,[35] which provided estimates for deposition velocities of O_3 and SO_2 over a temperate mixed forest in Canada, differences between modeled velocities were on the order of a factor of 2. In addition to model inter-comparisons, there is a need for evaluation of dry deposition parameterizations against field observations for a suite of atmospheric species[32,36] and ecosystems, which for Hg^0 are largely lacking.

To estimate Hg^0 emissions from soils and vegetative surfaces to the atmosphere, several empirical functions and models have been developed.[37–43] Parameterizations of soil emissions are based primarily on measured field fluxes and observed environmental drivers such as air and soil temperatures, solar radiation, soil moisture, and soil Hg content.[1] Several of these formulations have been implemented in CTMs, with modifications, for terrestrial surfaces. For example, in GEOS-Chem,[23] soil re-emission is parameterized following Zhang *et al.*,[39] in which re-emission of Hg^0 is a function of incident solar radiation at the ground surface. Additional approaches, such as that of the Global Terrestrial Mercury Model (GTMM), simulate Hg^0 re-emission from the soil organic carbon pools with which Hg^0 is associated.[44] Currently, due to knowledge gaps in a fundamental mechanistic understanding of Hg^0 exchange between air and soil and air and vegetation,[1,45] it is infeasible to implement a fully mechanistic surface-atmosphere exchange parameterization in CTMs.

In this study, we tested existing parameterizations of Hg^0 exchange implemented in CTMs by comparing model results to direct Hg^0 flux measurements at the ecosystem level (*i.e.*, including both soil and vegetation exchanges) at two sites for summer and winter seasons. Our comparison focuses on the commonly used dry gaseous Hg^0 deposition scheme from Zhang *et al.*[20] and a soil re-emission scheme implemented in GEOS-Chem.[24] We evaluated model performance against whole-ecosystem net exchange fluxes measured at a grassland site in Switzerland and at an Arctic tundra site in Alaska, U.S. The objectives of this study were to: (1) assess the performance of the current dry deposition and soil re-emission parameterizations in modeling net Hg^0 exchange fluxes; (2) characterize which model parameters most strongly influence modeled fluxes and how their adjustment improves agreement with field measured fluxes; and (3) provide suggestions for future treatment and further development of Hg^0 atmosphere-terrestrial surface exchange parameterizations in CTMs.

2. Parameterizations of Hg^0 atmosphere-terrestrial surface exchange examined

In most CTMs, Hg^0 dry deposition to and emission from terrestrial surfaces is parameterized separately (*i.e.*, de-coupled treatment). There are two major limitations of the de-coupled treatment. First, in this approach, dry deposition of Hg^0 is assumed to be independent of Hg content in the surface (top soils and/or leaves) where it gets deposited. However, coupled but complex parameterizations[31,46,47] are available, which account for this process by incorporating model parameters such as compensation point and emission potential of ground and leaf stomata. Second, photo-reduction of oxidized mercury (Hg^{II}), which enter leaf and ground surfaces *via* dry and wet deposition pathways and subsequent re-emission[44] in the form of Hg^0 is not taken into account in the de-coupled modeling framework. Given the lack of land use category (LUC)/site-specific measured values of the parameters involved the aforementioned processes, our study focuses on investigating the simpler de-coupled parameterization of Hg^0 exchange.

The resistance-based formulations of Zhang *et al.*[20] were used to model deposition flux of Hg^0 because they are the most up-to-date and widely used resistance-based deposition parameterizations. The framework of the Zhang *et al.*[20] model

follows the resistance analogy proposed by Wesely.[17] In both models, three parallel resistances to gaseous deposition are assumed: aerodynamic, boundary or quasi-laminar, and surface resistance. The resistance model[20] uses leaf area index (LAI) to scale Hg^0 uptake by foliage and uses updated formulations (that incorporate effects of LAI, relative humidity, and friction velocity) for non-stomatal (*e.g.*, cuticular) and ground deposition. The model allows selection of LUC parameters that are specific for grassland (*i.e.*, long grass), tundra, and other LUCs. The major resistance expressions in the Zhang *et al.*[20] parameterization are described in Section 2.1. To model soil re-emission of Hg^0, the base parameterization used in the current GEOS-Chem (v9-02) Hg model[24] was applied as described in detail in Section 2.2.

2.1. Modeling dry deposition of Hg^0

In global 3-D CTMs, the uptake of gaseous species at the surface is characterized by a downward dry deposition flux (F_d, ng m^{-2} h^{-1}) to be applied at the lowest model layer located at finite distance, z (m), from the surface. Vertical flux in the surface layer is assumed to be conserved for a species, and its dry deposition velocity (v_d, m s^{-1} or m h^{-1}) is calculated as $v_d = F_d(z)/C_z$, where C_z (ng m^{-3}) is gaseous concentration at height z. In CTMs that employ a resistance-based dry deposition parameterization, v_d for gaseous species such as Hg^0 is parameterized using the electrical resistance analogy[20] as:

$$v_d = \frac{1}{R_a + R_b + R_s} \quad (1)$$

where R_a is the aerodynamic resistance, R_b is the quasi-laminar sublayer resistance, and R_s is the bulk surface resistance. The term R_s in eqn (1) has two components: the stomatal resistance (R_{st}) and the non-stomatal resistance (R_{nst}). In the paper by Zhang *et al.*,[20] R_s is parameterized as:

$$\frac{1}{R_s} = \frac{1 - W_{st}}{R_{st} + R_m} + \frac{1}{R_{nst}} \quad (2)$$

where W_{st} is the fraction of stomatal blockage under wet conditions, and R_m is the mesophyll resistance. The R_{nst} term is parameterized by Zhang *et al.*[20] as:

$$\frac{1}{R_{nst}} = \frac{1}{R_{ac} + R_{gd}} + \frac{1}{R_{cut}} \quad (3)$$

where R_{ac} is the in-canopy aerodynamic resistance, R_{gd} is the ground resistance, and R_{cut} is the cuticular resistance. R_{gd} and R_{cut} are gaseous species dependent parameters. For any species i (except SO_2 and O_3), Zhang *et al.*[20] suggested the following scaling approach to calculate $R_x(i)$ ($R_x = R_{gd}$ or R_{cut}):

$$\frac{1}{R_x(i)} = \frac{\beta}{R_x(O_3)} + \frac{\alpha}{R_x(SO_2)} \quad (4)$$

where α and β are scaling factors for chemical species solubility and half-redox reactivity, respectively, suggested for Hg^0 to be $\alpha = 0$ and $\beta = 0.1$.[46] The expressions used to calculate the individual resistance terms shown in eqn (2) and (3) and the LUC-specific base resistance parameter values can be found in Zhang *et al.*[20] and references therein.

2.2. Modeling re-emission of Hg^0

In a recent study that employed stable Hg isotopes to measure exchange fluxes for the first time, the potential re-emission flux of Hg^0 from leaves was measured to be 30% in a forest canopy.[48] However, that study also reported a large uncertainty range (29–83%). Because of the current uncertainty in the re-emission flux and its temporal variation, we did not implement an immediate re-emission flux of Hg^0 from canopies in our model evaluation. However, we discuss this opportunity below as a part of our analysis of model performance whereby we selected to reduce stomatal Hg^0 uptake to achieve better model-to-measurement agreement.

In the original GEOS-Chem Hg model (described by Selin *et al.*[23]), the soil emission flux of Hg^0 was parameterized as a function of soil Hg concentration, solar radiation, and soil surface temperature based on the formulations by Zhang *et al.*[39] and Poissant and Casimir,[37] respectively. However, the current version of the GEOS-Chem Hg model[24] estimates the soil emission flux ($E_{soil\_GEOSChem}$ in ng m^{-2} h^{-1}) as a function of solar radiation as:

$$E_{soil\_GEOSChem} = \gamma C_{soil} \exp(1.1 \times 10^{-3} \times R_g) \quad (5)$$

where C_{soil} is the soil Hg concentration (ng g^{-1}) and R_g is the solar radiation flux at the ground (W m^{-2}). The scaling factor γ (1.2×10^{-2} g m^{-2} h^{-1}) is used to account for the global mass balance of the preindustrial model simulation. Selin *et al.*[23] used the following expression to calculate R_g as functions of solar radiation (SR, W m^{-2}) at the top of the canopy and LAI:

$$R_g = SR \exp\left(\frac{-\mu LAI}{\cos\theta}\right) \quad (6)$$

where θ is the solar zenith angle and $\mu = 0.5$ is an extinction coefficient assuming random leaf angle distributions.

3. Methods

3.1. Measurement data

Field-based micrometeorological net exchange fluxes of Hg^0 used for model evaluation were measured in two ecosystems, a grassland and a tundra, which correspond to LUC categories "long grass" and "tundra", respectively in the Zhang *et al.*[20] parameterization. The Hg^0 exchange flux data set at a subalpine grassland site at Früebüel (47° 6′ N, 8° 32′ E, elevation of 1000 m above sea level (m a.s.l.)) in central Switzerland were acquired by and published in Fritsche *et al.*[49] The measurement location is a research site of ETH Zürich, located in the temperate continental climate with the mean annual precipitation of 1200 mm and a mean annual air temperature of 7 °C. The area of the site is 9 ha with a micrometeorological tower built in the center. A detailed description of the site is provided by Fritchse *et al.*[49] At this site, Hg^0 exchange fluxes were measured over a full year (September 2005 to August 2006). The second site at which exchange fluxes were measured was Toolik Field Station.[12] This Arctic tundra site is located in the northern foothills of the Brooks Range, Alaska, U.S. (68° 38′ N, 149° 38′ W, elevation of 760 m a.s.l.). The site, which is representative

of interior tundra, is located 200 km inland from Deadhorse near the Arctic Ocean.[12,50] The site is bordered by Toolik Lake to the north. Typical mean annual precipitation and mean annual temperature at the site are 312 mm and −8 °C.[51] Hg^0 flux exchange measurements were conducted at the Toolik Field Station site from September 2014 to September 2016. We used exchange flux measurements and meteorological data for the year 2016 from this site for model evaluation. At both sites, the aerodynamic flux method was used to quantify surface-atmosphere fluxes of Hg^0.[12,49] Briefly, at the grassland site, Hg^0 concentrations were measured at five heights above the soil surface (0.20, 0.27, 0.94, 1.58, and 1.70 m). The gradient fluxes were calculated for the following five height pairs: 0.2/1.58, 0.27/1.58, 0.27/1.7, 0.94/1.7, and 0.2/0.94 m, and the reported fluxes were the median of these fluxes.[49] At the tundra site, fluxes were estimated using Hg^0 concentrations measured at heights of 0.61 m and 3.63 m above the soil surface.[12] For both sites, data were hourly averages for atmospheric Hg^0 concentrations and Hg^0 net exchange fluxes, and corresponding values of wind speed, friction velocity, air temperature, surface soil temperature, solar radiation, atmospheric pressure, relative humidity, and Monin–Obukhov length. For analysis of 24 h temporal patterns (further referred to as *diel variation*), the aforementioned measured variables were averaged hourly for July and August (at both sites) and for December (grassland site) and January (tundra site). The choice of these months for model simulations primarily stems from availability of measured net exchange data for a given season at each site. In addition, to reduce noise in measured flux variability and to better track the diel variation of Hg^0 fluxes, a 5 hour moving average filter was used for measured Hg^0 fluxes. The need for temporal averaging and filtering was due to the large variability in measured 1/2 hour flux data, which stems from difficulties in measuring small exchange fluxes against a large background concentration as documented for several micrometeorological Hg^0 flux data sets (*e.g.*, Fritsche *et al.*[49]). For soil Hg^0 emission model simulations, we used measured surface soil Hg concentrations of 100 ng g^{-1} at the grassland[49] and tundra[52] sites.

3.2. Model evaluation

To evaluate the performance of the base parameterizations developed by Zhang *et al.*[20] and Song *et al.*,[24] LUC-specific simulations were performed. Hourly averaged meteorological and atmospheric concentrations from the two sites were used as model inputs. To account for seasonal variability in the modeling analysis, simulations were conducted for typical summer and winter meteorological conditions for each of the two ecosystems using averaged hourly conditions for July, August, and December measurements at the grassland site and July, August, and January measurements at the tundra site. The model was run using these hourly averaged environmental parameters, which were assumed to be representative of the hourly conditions for a typical day in a given month. At the grassland site, a LAI of 5.0 m^2 m^{-2} was used for July and August month simulations derived from monthly averaged MODerate resolution Imaging Spectroradiometer (MODIS)-Terra.[53] At the tundra site, average LAIs of 1.5 and 2.0 m^2 m^{-2} were used for July and August base model simulations, respectively.

Agreement between the measured and modeled exchange fluxes was evaluated using degree of agreement (d), calculated using eqn (7):

$$d = 1 - \frac{\sum_{i=1}^{n} (O_i - M_i)^2}{\sum_{i=1}^{n} (|O_i| + |M_i|)^2} \quad (7)$$

where O_i is the observed net flux (ng m^{-2} h^{-1}), M_i is the modeled net flux (ng m^{-2} h^{-1}), and n is the number of observations. A d-value closer to one indicates better agreement of modeled values with observed values. Based on the performance of the base model, adjustments to the default model parameters were performed through application of adjustment factors. The adjustments of model parameters primarily provided a sensitivity analysis with the objective to assess which parameter adjustments resulted in the most relevant changes (in both magnitude and direction) and best agreement with measured field-based fluxes. Model response (referred to as "adjusted model") to these adjustments was assessed and is discussed in detail, and suggestions are provided for the future treatment of net exchange processes of Hg^0 in CTMs.

4. Results and discussion

In Sections 4.1 and 4.2, measured ecosystem-level atmosphere-terrestrial surface exchange fluxes of Hg^0 from both sites are compared with modeled net exchange fluxes using the base parameterizations. In Sections 4.3 and 4.4, sensitivity simulations were performed to assess how changing default model parameters changed the modeled Hg^0 fluxes (magnitude and direction) to best match observed fluxes. In Section 4.5, growing season vegetation Hg uptake was calculated using the base and adjusted parameterizations and compared with observed Hg accumulation in plant leaves to serve as an additional model constraint.

4.1. Evaluation of summer base model net exchange fluxes

4.1.1. Temperate grassland site in Switzerland. Fig. 1 shows modeled fluxes, computed using the base model with the default dry deposition and re-emission parameterizations, and hourly averaged measured fluxes for two summer months. Throughout this paper, emission and deposition fluxes are denoted by positive and negative signs, respectively.

Diel Hg^0 patterns of modeled F_{net} were primarily controlled by the surface resistance term (R_s in eqn (1)), which is composed of stomatal and non-stomatal uptake. Of the two deposition pathways, stomatal uptake dominated over non-stomatal uptake. Strongly increased net deposition of Hg^0 in the daytime compared to nighttime deposition is largely attributable to increased stomatal uptake during the daytime (R_{st} term in eqn (2)). The sub-model that calculates R_{st} for all gaseous species, including Hg^0, is an inverse function of photosynthetically active radiation (PAR) as well as a function

of air temperature, water-vapor deficit, and leaf water potential (see eqn (6) in Zhang *et al.*[20] for details). Hence, the magnitude of the diel variation in R_{st} is strongly driven by solar radiation. The lowest R_{st} value corresponding to the highest net deposition is typically observed at around midday when PAR is maximum. Comparison between measured and modeled F_{net} suggests that while the base model was able to capture the observed diel pattern of fluxes, it considerably overestimated net deposition of Hg^0 during the daytime. In addition, measured F_{net} showed a nighttime deposition of Hg^0 in the range of −1.2 to −3.3 ng m^{-2} h^{-1}, which the model was unable to reproduce and instead predicted nighttime fluxes near zero (*i.e.*, neither net deposition nor net emission).

Measured daytime F_{net} exhibited a bimodal variation having increased deposition in the mornings and afternoons and reduced net deposition at midday, which may be caused by either midday leaf stomatal closure or by increased soil Hg^0 emissions during midday when solar radiation and soil surface temperature are highest (both positively correlate with soil Hg^0 emissions[2]). The base model was able to reproduce the observed bimodal flux distribution during daytime, albeit with a time lag of 1 to 2 hours. However, the absolute differences in measured and modeled F_{net} are large throughout the daytime. For example, the mean measured and modeled daytime F_{net} (07:00 to 20:00 LT) were −4.4 ng m^{-2} h^{-1} and −13.8 ng m^{-2} h^{-1}, respectively, demonstrating that the base model overestimated the measured deposition by a factor >3. In addition, during the nighttime (21:00 to 06:00 LT), the base model largely failed to reproduce the observed net deposition resulting in model underestimation of mean nighttime net deposition of 1.2 ng m^{-2} h^{-1}. On a daily basis, the base model overestimated the measured F_{net} by a factor of approximately 2.5 in summer (cumulative measured F_{net} of −87.5 ng m^{-2} d^{-1} *vs.* −205.4 ng m^{-2} d^{-1} predicted by the base model).

4.1.2. Arctic tundra site at Toolik Field Station, Alaska. Comparison between the modeled and hourly averaged measured F_{net} for the summer months (July and August of 2016) at the tundra site are shown in Fig. 2. Field measurements exhibited net deposition in the morning and afternoon F_{net}, while the midday F_{net} exhibited net emission. Total daytime fluxes (04:00 to 23:00 LT) exhibited deposition smaller than at the grassland, averaging −0.4 ng m^{-2} h^{-1}. Similar to the grassland ecosystem, modeled net deposition fluxes were substantially higher throughout daytime (−2.7 ng m^{-2} h^{-1}). During the short nighttime period (00:00 to 03:00 LT), measured F_{net} was dominated by a strong Hg^0 deposition (mean of −2.8 ng m^{-2} h^{-1}), which the base model was unable to reproduce (mean of −0.2 ng m^{-2} h^{-1}). Comparison between measured and modeled fluxes at nighttime shows that the base model underestimated measured net deposition by 2.6 ng m^{-2} h^{-1}. On a daily basis, the base model overestimated the measured F_{net} (*i.e.*, net deposition) by a factor approximately 3 in summer (cumulative measured F_{net} of −18.4 ng m^{-2} d^{-1} *vs.* −54.6 ng m^{-2} d^{-1} predicted by the base model).

4.2. Evaluation of winter base model net exchange fluxes

In winter, modeled F_{net} fluxes at both sites largely lacked diel flux patterns whereas measured fluxes exhibited diel variations (Fig. 3). Overall, the temperate grassland exhibited measured net Hg^0 deposition in the range of −0.2 to −5.3 ng m^{-2} h^{-1} during the nighttime (18:00 to 08:00 LT), while during the afternoon (14:00 to 16:00 LT) there was a small net emission (approximately 1.4 ng m^{-2} h^{-1}; Fig. 3A). In winter at the tundra site (Fig. 3B), measured F_{net} exhibited a small net deposition for most of the day with no clear differences between nighttime and daytime fluxes and with hourly fluxes ranging from −1.1 ng m^{-2} h^{-1} (small net deposition) to 0.9 ng m^{-2} h^{-1} (small net emission). Note that for winter months, we assumed LAI of 0 m^2 m^{-2} (*i.e.*, no vegetation activity), but did not implement

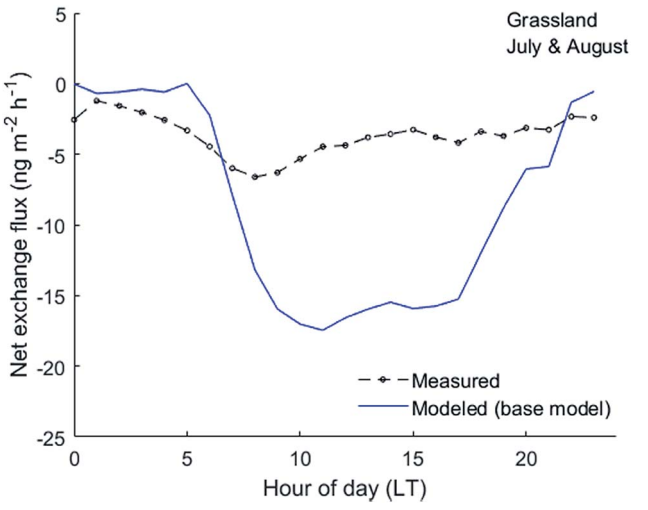

Fig. 1 Comparison of modeled (blue, solid; base model) and averaged diel measured (black, dashed) net exchange fluxes of Hg^0 (F_{net}) at the grassland site (Früebüel, Switzerland) in summer of 2006 (LT = local time).

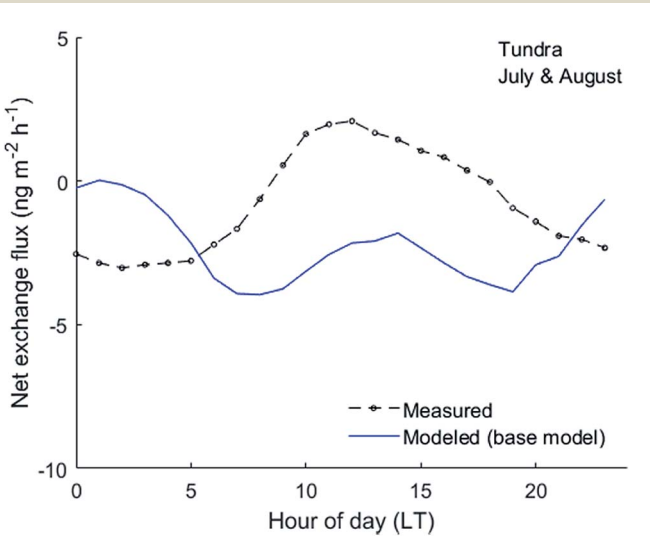

Fig. 2 Comparison of modeled (blue, solid; base model) and averaged diel measured (black, dashed) net exchange fluxes of Hg^0 (F_{net}) at the Arctic tundra site (Toolik Field Station, Alaska, U.S.) in summer of 2016.

any further processes related to snow cover. At both sites, the base model was unable to reproduce the small measured net deposition and consistently produced a small rate of net Hg^0 emissions during both daytime and nighttime. In winter months, cumulative modeled net daily emissions at the grassland and tundra sites were 18.9 and 23.4 ng m^{-2} d^{-1}, respectively. In comparison, measured net daily deposition was −34.7 and −5.2 ng m^{-2} d^{-1}, respectively, at the two sites.

4.3. Model response to adjusted deposition parameterization in summer

The measurement-model comparisons shown in Fig. 1, 2, and 3 suggest that in order to improve the performance of modeled exchange, three major components in the net exchange (*i.e.*, deposition and emission) models need to be addressed. First, net nighttime Hg^0 deposition observed at both sites is largely lacking in model simulations, suggesting that the current Hg^0 deposition scheme, which is strongly driven by stomatal Hg^0 uptake, should employ stronger deposition *via* non-stomatal pathways that are active during night as well (either cuticular, R_{cut}, or ground, R_{gd}, resistance terms in eqn (3)). Second, the modeled daytime Hg^0 uptake needs to be reduced substantially, because daytime deposition is over-predicted in the modeled F_{net} by a factor of up to 5 (summer at the grassland site). This adjustment can be implemented either by increasing the stomatal resistance R_{st} term in eqn (2) or by application of a Hg^0 re-emission factor of stomatal Hg^0 uptake, as suggested by Yuan *et al.*[48] We selected the first option, although both methods would lead to similar reductions in stomatal Hg^0 uptake. Third, further improvement in model *vs.* measurement agreement can be reached by adjusting the soil Hg^0 re-emission scheme. In Sections 4.3.1 and 4.3.2, we discuss a sensitivity analysis and modeled flux responses to adjustment of the corresponding resistance parameters, R_{st}, R_{cut}, and R_{gd}.

4.3.1. Model response to reduced stomatal uptake. Modeled diel flux patterns in the default dry Hg^0 deposition model are driven by stomatal Hg^0 uptake, which generally accounts for over 90% of the modeled daytime Hg^0 deposition resulting in strong over-prediction of daytime deposition, as illustrated above. Minimal stomatal resistance (r_{stmin}) is one of the primary controlling variables in R_{st} (the expressions for estimating these two terms are discussed in detail by Zhang *et al.*[20] and references therein). In the Zhang *et al.*[20] dry deposition parameterization, default parameter values were suggested for r_{stmin} for different LUCs, including a default value r_{stmin} of 100 s m^{-1} for long grass. To reduce the stomatal uptake of Hg^0 during the daytime, we performed a set of sensitivity tests by varying the default r_{stmin} value over a wide range (100 to 800 s m^{-1}) and examining the corresponding responses to the modeled net exchange fluxes. For the grassland site, we found that an increase in the default r_{stmin} value by a factor of seven led to significant reduction of daytime Hg^0 deposition and reasonably good agreement between the measured and modeled daytime fluxes, as shown in Fig. 4.

For the tundra site, a similar approach was taken to examine the sensitivity of net exchange changes to the r_{stmin} value. The default parameter value for r_{stmin} was 150 s m^{-1} for the tundra LUC[20] and r_{stmin} was varied from 150 to 1050 s m^{-1}. We found that a five-fold increase in the default r_{stmin} (*i.e.*, to 750 s m^{-1}) led to an improved performance of the base model Hg^0 deposition during the day (Fig. 4B). Any further increase in the r_{stmin} value caused worsening of model performance in the nighttime. Hence, comparisons between the base model and adjusted model simulations with increased stomatal resistance by factors of 7 (temperate grassland) and 5 (Arctic tundra) suggest that the dry deposition model is sensitive to changes in r_{stmin} such that large adjustments to r_{stmin} substantially improved the agreement between measured and modeled net exchange fluxes during the daytime for both ecosystems in summer months. For example, at the grassland site, daytime net Hg^0 deposition with the adjusted r_{stmin} parameterization deviated on average by 1.9 ng m^{-2} h^{-1} from the measured fluxes, while deviations from the unadjusted or base model averaged 9.4 ng m^{-2} h^{-1}. At the tundra site, daytime net Hg^0 deposition with the adjusted r_{stmin} value deviated on average by 0.02 ng m^{-2} h^{-1} from measured fluxes compared to 2.3 ng m^{-2} h^{-1} for the base model.

4.3.2. Model response to combined effects of increased ground and cuticular uptake and reduced stomatal uptake. In

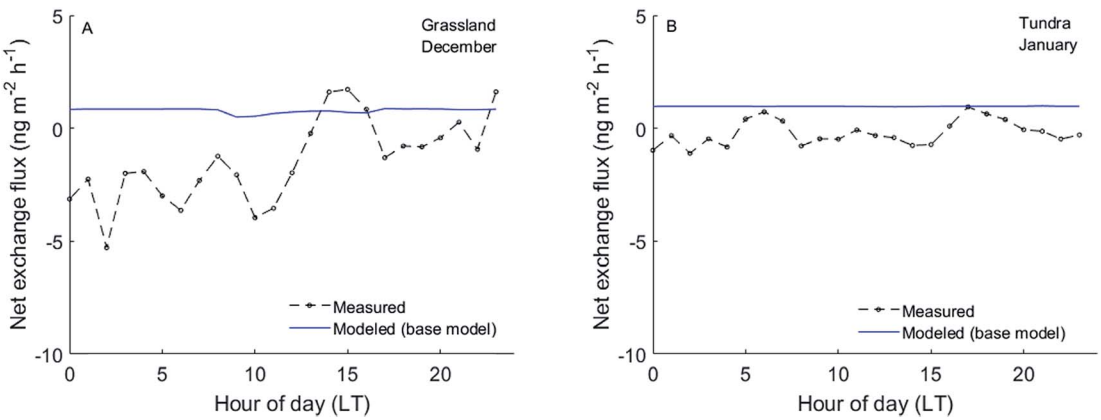

Fig. 3 Comparison of modeled (blue, solid; base model) and averaged diel variations of measured (black, dashed) net exchange fluxes of Hg^0 in winter at: (A) the temperate grassland site in December 2005 and (B) the Arctic tundra site in January 2016.

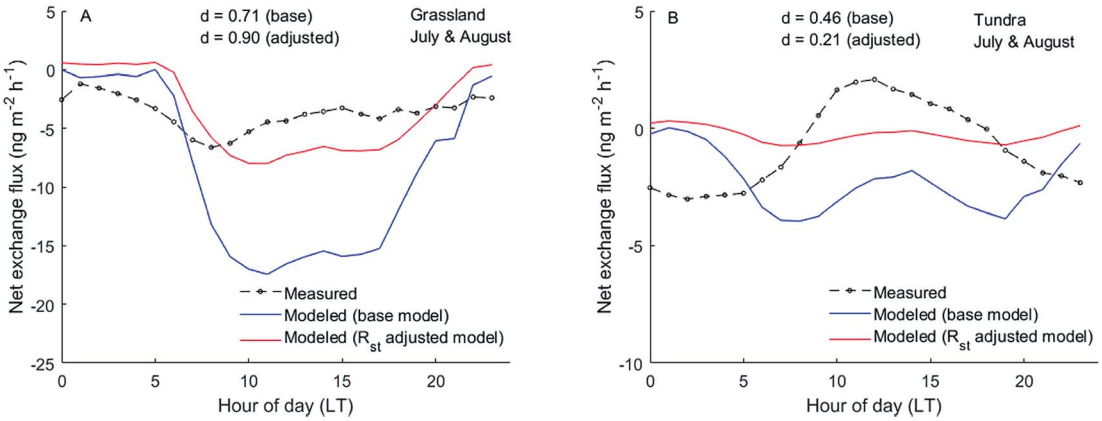

Fig. 4 Model response to reduced stomatal uptakes of Hg^0 and comparison of modeled and measured net exchange fluxes of Hg^0 in summer at: (A) the temperate grassland site, and (B) the Arctic tundra site.

the temperate grassland and Arctic tundra sites, measured F_{net} exhibited a net Hg^0 deposition during the nighttime, which the base model and the stomatal resistance-adjusted model were largely unable to reproduce. Increased nighttime Hg^0 deposition (*i.e.*, in the absence of significant stomatal uptake) observed in the flux measurements can be simulated either by increasing the ground (R_{gd}) and/or the cuticular (R_{cut}; *i.e.*, to the leaf surface) uptake of Hg^0, or by reducing soil re-emission fluxes (Section 4.3.3). We first increased the ground and cuticular uptake along with the implemented reduced stomatal uptake described above, and show the resulting changes in model behavior in Fig. 5.

For the grassland site, we first tested the sensitivity of adjusting the default parameters for cuticular resistance (dry) (R_{cutdO_3}) and ground resistance (dry) R_{gdO_3}, which in the base model were 4000 and 200 s m^{-1}, respectively, for the long grass LUC.[20] Note that the values for these resistance parameters are based on O_3 deposition assuming dry conditions. A sensitivity test was performed using the following ranges for R_{cutdO_3} and R_{gdO_3}, respectively: 500–4000 s m^{-1} and 50–200 s m^{-1}. We found that reductions in the default parameter values for R_{cutdO_3} and R_{gdO_3} by factors greater than four resulted in insignificant improvements in nighttime model performance (Fig. 5A). Also, such increases substantially worsened daytime model performance for both summer months. Thus, we applied factors of four reductions to the base values of both of these parameters.

Similarly, for the tundra site, we first tested the sensitivity of adjusting the default parameters for R_{cutdO_3} and R_{gdO_3}, which were 8000 and 500 s m^{-1}, respectively, in the Zhang *et al.*[20] model. A sensitivity test was performed using the following ranges for R_{cutdO_3} and R_{gdO_3}, respectively: 500–8000 s m^{-1} and 50–200 s m^{-1}. We determined that factors of two and three decreases in the base values of R_{cutdO_3} and R_{gdO_3}, respectively, produced an exchange flux pattern that exhibited small net nighttime deposition (Fig. 5B).

Implementation of fractional re-emission of Hg^0 from leaf surfaces could further optimize model performance. Even though evidence from Hg^0 flux measurements and stable isotope data[7,10,48] support occurrence of such Hg^0 re-emission, the estimated uncertainty in the fraction of Hg^0 re-emission from leaf surfaces is large (29–83%) and the proposed 30% average re-emission[48] would not fully address the current overestimation in canopy Hg^0 uptake. Therefore, in this evaluation we did not apply a fractional re-emission loss from plant surfaces. However, such a fractional re-emission loss could work in a fashion similar to the reduced stomatal uptake parameters and improve the agreement between measured and modeled fluxes.

Still, our simulations suggest that adjustments of resistance parameters alone (*i.e.*, stomatal, cuticular, and ground) cannot satisfactorily reproduce the measured fluxes even though the increased stomatal resistance led to a large improvement in modeled daytime fluxes. In particular, daytime Hg^0 deposition is overestimated at midday. To address the discrepancy a soil Hg^0 re-emission function was added to the deposition model as described next.

4.3.3. A revised soil Hg^0 re-emission parameterization and associated model response. Soil re-emission of Hg^0 is often parameterized as an exponential function of solar radiation and surface temperature.[3,39,54,55] Based on field measurements it is also apparent that nighttime soil Hg^0 re-emission is generally low and often negligible. We suggest that implementing a larger daytime soil Hg^0 emission along with a nighttime Hg^0 emission of zero would improve the agreement between modeled and measured diurnal patterns of exchange fluxes. The existing soil re-emission parameterization in GEOS-Chem implemented according to the formulation of Zhang *et al.*[39] exhibited little diurnal variation in re-emission (Fig. S1†). We achieved the needed changes (larger daytime emission and smaller nighttime emission) by modifying the empirical soil Hg^0 re-emission parameterization of Eckley *et al.*[2] in which the soil re-emission flux is a function of solar radiation:

$$E_{soil\_Eckley} = 10^{[0.709+0.119\log(C_{soil})+0.137\log(\text{solar radiation})]} \quad (8)$$

To better account for diurnal variability in soil Hg^0 re-emission fluxes and include the effect of vegetative shading

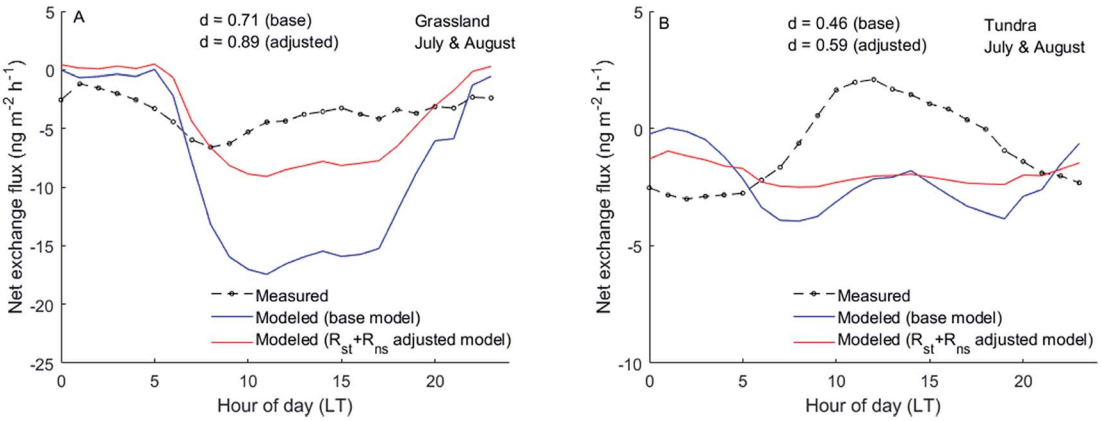

Fig. 5 Model response to increased cuticular and ground uptake, and reduced stomatal uptake, of Hg^0, and comparison of modeled and measured net exchange fluxes of Hg^0 at: (A) the temperate grassland site, and (B) the Arctic tundra site.

on solar radiation reaching the soil surface, we modified eqn (8):

$$E_{\text{soil\_new}} = 10^{\left[0.709+0.119\log(C_{\text{soil}})+0.137\log\left(R'_{\text{g}}\right)\right]} \times a^{-1} \sin\frac{\pi t}{D} \quad (9)$$

where $E_{\text{soil\_new}}$ is soil re-emission flux in ng m^{-2} h^{-1}, C_{soil} is soil Hg concentration in μg g^{-1}, and R'_{g} is adjusted solar radiation at the soil surface, which accounts for vegetative shading, in W m^{-2}.

$$R'_{\text{g}} = \text{SR}\exp(-\mu\text{LAI}) \quad (10)$$

SR is the solar radiation on top of the canopy. We used hourly values of SR in all model simulations. In eqn (9), a sinusoidal function is added consistent with the canopy light attenuation formulation,[56] where D is duration (in hour) between sunrise and sunset, and t is time (in hour) of daylight hours. We estimated the solar radiation at the ground (R'_{g}) without normalizing the exponential term by solar zenith angle as shown in eqn (6). Instead, the expression for R'_{g} (eqn (10)) is consistent with the formulation given by Kocman and Horvat.[57] We note that while eqn (8) provides the basis for eqn (9), as can be seen from Fig. S1,† implementing the sin function greatly improved the diel pattern of the modeled soil re-emission fluxes, which could not be captured by eqn (8). Using eqn (9) also enables the smooth transition between nighttime and daytime re-emission fluxes, which would not be achieved otherwise.

A sensitivity test was conducted for both sites to determine the value of the coefficient a in eqn (9) that produced the best-fit modeled soil flux values as compared to measured soil flux values. Following eqn (8), we simulated net exchange fluxes using reduced nighttime and increased daytime soil Hg^0 re-emission for summer months at the grassland and tundra sites. For both sites in summer, we found that a value of a of 1.5 produced the best agreement between the modeled and measured F_{net} (Fig. 6). The major outcome of modifying the previous soil re-emission parameterization was a substantial improvement in model ability to reproduce the observed diel pattern of F_{net}, in particular by eliminating nighttime soil re-emission and substantially increasing daytime emissions (see also Fig. S1†). The resulting pattern of modeled soil re-emission fluxes is consistent with measured fluxes reported in the literature. For example, Agnan *et al.*[3] showed that several studies reported a strong diurnal pattern in measured flux. The authors

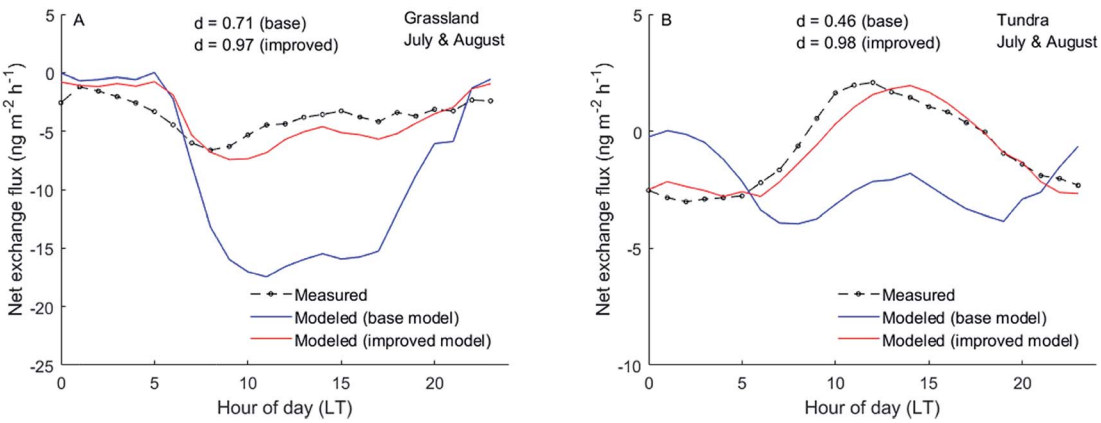

Fig. 6 Model response to reduced nighttime and increased daytime soil re-emission and revised resistance parameters, and comparison of modeled and measured net exchange fluxes of Hg^0 in July and August at: (A) the temperate grassland site, and (B) the Arctic tundra site.

Table 1 Mean measured and modeled F_{net} (ng m^{-2} h^{-1}) at the grassland and tundra sites

Season	Measured	Modeled (base)	Modeled (improved)	*d*-Value[a]
(A) Grassland site				
Mean F_{net} (daytime)				
Summer (July & August)	−4.4	−13.8	−5.6	
Winter (December)	−1.0	0.7	−1.4	
Mean F_{net} (night time)				
Summer (July & August)	−2.6	−1.2	−1.3	
Winter (December)	−1.7	0.9	−1.4	
Mean F_{net} (daily)				
Summer (July & August)	−3.6	−8.6	−3.8	0.97 (0.71)
Winter (December)	−1.4	0.8	−1.4	0.74 (0.07)
(B) Tundra site				
Mean F_{net} (daytime)				
Summer (July & August)	−0.4	−2.7	−0.6	
Winter (January)	−0.6	1.0	−0.2	
Mean F_{net} (night time)				
Summer (July & August)	−2.8	−0.1	−2.4	
Winter (January)	−0.2	1.0	−0.2	
Mean F_{net} (daily)				
Summer (July & August)	−0.8	−2.2	−0.9	0.98 (0.46)
Winter (January)	−0.2	1.0	−0.2	0.52 (0.25)

[a] Values in parentheses indicate base model *vs.* measurement agreement.

compiled flux data from 132 studies, and reported that 65 of those studies (the large majority of which were dynamic flux chamber studies) found a positive correlation between measured Hg^0 flux and solar radiation (Table S1,† Agnan *et al.*[3]).

As a result of the adjustment in emission fluxes, the ratio between modeled and measured daily sum of F_{net} at the temperate grassland site decreased from factors of approximately 2.3 to 1.1 (improved model) in summer (Fig. 6A; diel mean modeled net fluxes of −3.6 *vs.* measured fluxes of −3.8 ng m^{-2} h^{-1}). Degree of agreement (*d*) values between (diel) modeled and observed fluxes also support the improvement in model performance (*i.e.*, 0.97 *vs.* 0.71 for summer). The improvement in both the ratios and *d*-values demonstrates that revising the soil re-emission function can significantly improve the agreement between modeled and measured Hg^0 fluxes (Table 1).

For the Arctic tundra site, we found that the absolute difference between the mean diel modeled and measured fluxes (net deposition) decreased from 1.5 to 0.1 ng m^{-2} h^{-1} in summer, and the *d*-values of the base *vs.* adjusted model were 0.98 *vs.* 0.46; Fig. 6B. Table 2 presents the adjustment factors used to revise the base resistance parameter values for the two sites.

4.4. Model response to revised dry deposition and soil re-emission parameterizations in winter

For winter months, we performed the same adjustments for the dry deposition model, and show the results of these adjustments in Fig. 7. The results indicate that in winter months with sub-zero air temperature and snow on the ground, revisions of these resistance terms of dry deposition had no discernable effect in improving the agreement between measured and modeled exchange fluxes. However, the modeled fluxes of both the base simulation and the adjusted simulation largely replicated a lack of strong diel patterns in measured Hg^0 fluxes.

Neither simulation, however, is able to replicate an observed net Hg^0 sink under snow cover. We suggest adding a net soil Hg^0 sink along with eliminating re-emissions under snow, in agreement with field studies.[12,58] We also recommend decoupling wintertime fluxes from variability imposed by solar radiation and temperature. Fig. 8 shows how turning off soil re-emission (both in the day and at night) at both sites and adding

Table 2 Base and revised resistance parameter values (Zhang *et al.*[20])

Ecosystem	Resistance parameter	Sensitivity simulation	Base value (s m^{-1})	Revised base value (s m^{-1})
Grassland	r_{stmin}	Stomatal	100	700
	R_{cutdO_3}	Cuticle	4000	1000
	R_{gdO_3}	Ground	200	50
Tundra	r_{stmin}	Stomatal	150	750
	R_{cutdO_3}	Cuticle	8000	4000
	R_{gdO_3}	Ground	500	167

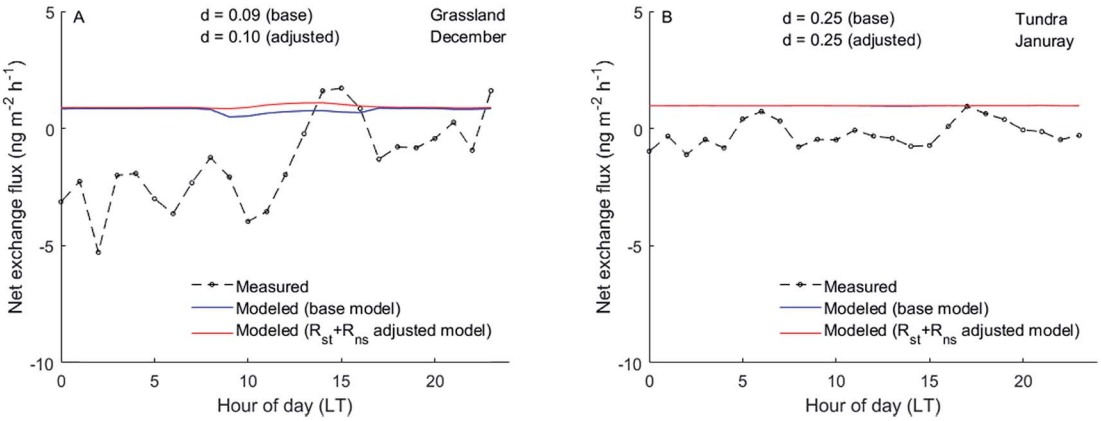

Fig. 7 Model response to reduced stomatal uptake and increased cuticular and ground uptake and comparison of modeled and measured net exchange fluxes at: (A) the grassland site in December 2006, and (B) the tundra site in January 2016.

a net soil Hg^0 sink (*e.g.*, on the order of 1 ng m^{-2} h^{-1}) at the grassland site led to the best agreement between measured and modeled net Hg^0 fluxes. Even still, the agreement between modeled and measured fluxes at both sites is modest (Table 1), possibly due to measurement issues of detecting small fluxes during the winter when stable atmospheric conditions make such measurements challenging.[12]

4.5. Seasonal mercury accumulation in leaves estimated using the adjusted deposition model parameterization

An additional, independent constraint of Hg^0 deposition can be achieved by comparing foliar Hg^0 uptake based on modeled stomatal and cuticular uptake to leaf Hg content measured in the field. Several studies have documented that during the growing season, atmospheric Hg^0 uptake in leaves results in increasing leaf Hg content over time.[59–61] Other studies, in particular using stable isotope analysis, have confirmed that foliar Hg is primarily derived of atmospheric Hg^0 uptake.[7,10] To evaluate how our proposed changes in stomatal and cuticular leaf resistance terms impact foliar Hg^0 accumulation, we estimated seasonal (April to August) Hg accumulation in vegetation at the grassland site for both the base and adjusted model parameterizations. The following expression was used to estimate the leaf Hg concentration (C_{Hgleaf}):

$$C_{Hgleaf}\ \left(\text{ng g}^{-1}\right) = F_{dep(st+cut)} \times t_L \times SLA \times \frac{1}{LAI} \qquad (11)$$

where $F_{dep(st+cut)}$ is the net dry deposition flux of Hg^0 (ng m^{-2} d^{-1}) due to leaf uptake *via* stomatal and cuticular pathways, t_L is the duration of the growing season in days, and SLA is the specific leaf surface area (leaf surface area per mass: m^2 g^{-1}). Because *Dactylis glomerata* L. is one of the dominant plant species at the Früebüel grassland site, we used a SLA value of 0.017 m^2 g^{-1} for this species[62] in eqn (11). Monthly averaged LAI values obtained from MODIS-Terra database[53] for each growing season month were used. To calculate deposition fluxes, the average measured atmospheric Hg^0 concentration[49] for each growing season month was used.

Comparison between seasonal Hg accumulation using the base model and the adjusted model (Fig. 9) supports the findings shown earlier that the base model parameterization strongly overestimates Hg^0 uptake. The base model-estimated tissue Hg concentration is 164 ng g^{-1}, which is much higher

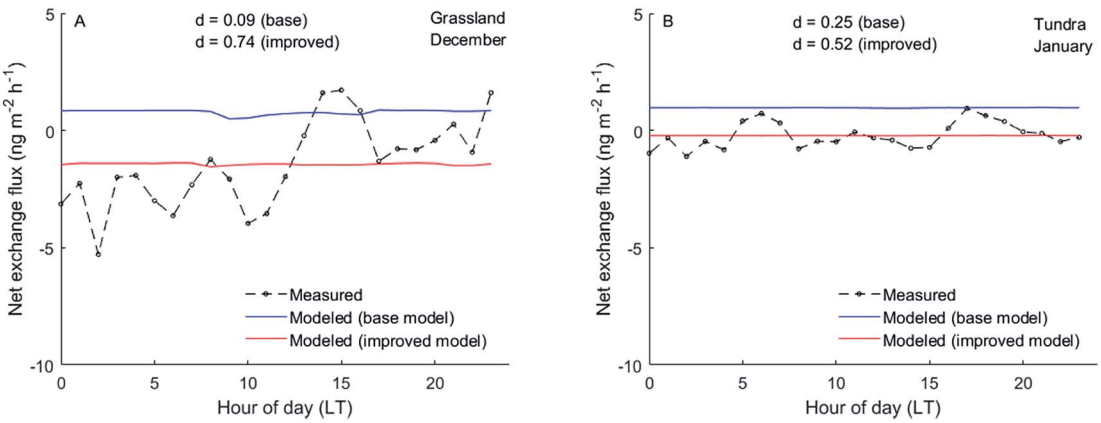

Fig. 8 Model response to reduced soil re-emission and revised resistance parameters, and comparison of modeled and measured net exchange fluxes of Hg^0 at: (A) the grassland site in December 2005, and (B) the tundra site in January 2016.

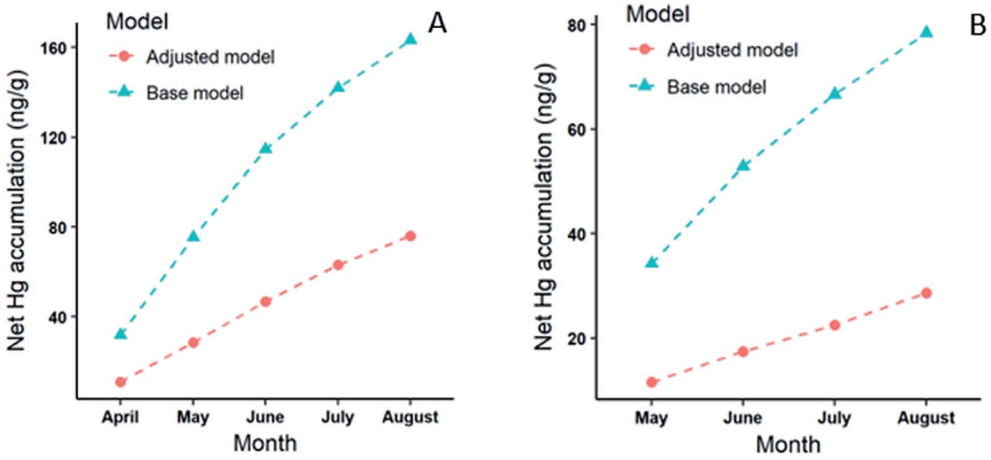

Fig. 9 Growing season Hg accumulation in: (A) *Dactylis glomerata* L. at the grassland site, and (B) *Betula nana* L. at the tundra site using the base and adjusted dry deposition models.

than leaf Hg concentrations commonly measured across ecosystems in temperate regions (21–78 ng g^{-1}; Wang *et al.*).[63] Using the adjusted deposition model parameterization with increased stomatal resistance (*i.e.*, reduced leaf Hg^0 uptake), we estimated a growing season tissue Hg concentration of 76 ng g^{-1}. This estimated value is comparable to commonly reported leaf and litterfall tissue concentrations in remote ecosystems in temperate regions.[63] A similar approach was taken to estimate the modeled growing season leaf tissue Hg concentration at the tundra site assuming *Betula nana* L., a shrub species, is the major species by biomass at the site. The adjusted model-derived leaf tissue concentration was found to be 29 ng g^{-1}, which compares well with measured leaf and litterfall concentrations of 25 ng g^{-1} at Toolik Field Station.[64]

5. Implications for Hg CTM models

Based on the evaluation presented here, the proposed adjustments to certain deposition parameters could improve regional and global CTMs that use resistance-based schemes to estimate dry deposition fluxes of Hg^0 at grassland and tundra LUCs, which together account for approximately 48% of vegetative surfaces globally.[65,66] The revised deposition parameters and re-emission scheme could be implemented in CTMs in scaling up the measurement site-LUC to 100% of the grid box land fraction using surface parameters (*e.g.*, LAI, roughness height, resistance terms) of the measurement site. This approach was applied by Silva and Heald[67] to improve the agreement between modeled and measured deposition velocities of O_3 at the global scale. Additional flux measurements are needed to optimize simulated Hg^0 atmosphere-surface exchange for other LUCs. In this study, we viewed the performance of the global/regional Hg model separately from the performance of the resistance-based deposition and empirical soil re-emission schemes. In practice, in CTMs, various biogeochemical processes (*e.g.*, dry and wet deposition, primary and secondary emissions, oxidation–reduction, photochemistry, *etc.*) are optimized to achieve a reasonable match to atmospheric Hg^0 concentration observations. We argue that additional improvement in CTM performance could be achieved by incorporating improved deposition and re-emission parameterizations of Hg^0.

6. Conclusion

To our knowledge, this is the first direct performance evaluation of Hg^0 net exchange parameterizations commonly used in CTMs with ecosystem level micrometeorological net exchange flux measurements. We evaluated how the major resistance terms affect modeled Hg^0 exchange and how they can be optimally parameterized to simulate measured net exchange fluxes. The base parameterizations overestimated measured net Hg deposition by factors of 3–4 in summer, led to unrealistically high tissue concentrations during the growing season, and did not simulate the strong diel variation in observed fluxes, with net nighttime deposition and net daytime Hg^0 volatilization.

The sensitivity analyses suggest the following LUC-specific recommendations for improvement in modeling Hg^0 exchange using resistance-based approaches. First, we suggest that stomatal resistance be increased several times to reduce bias in overestimating Hg^0 uptake. In the two ecosystems we studied the best performance was achieved through reduction of stomatal uptake by a factor of 7 (grassland) and 5 (tundra). Second, we suggest reductions in cuticular resistance by factors 4 (grassland) and 2 (tundra), and reductions in ground resistance by factors 4 (grassland) and 3 (tundra). Finally, we propose a new soil re-emission parameterization that simulates observed increased diel variations in Hg^0 fluxes and zero fluxes at nighttime. These recommendations should be further tested by incorporation of the suggested changes in flux parameters/parameterizations into regional and global models that simulate other important processes involved in environmental cycling of Hg (such as primary emissions, re-emissions from oceans, chemistry, *etc.*) and comparison with measured atmospheric Hg^0 concentrations. Additional ecosystem-level Hg^0 exchange and foliar uptake measurements will enable constraints on model parameters and improvement in Hg CTM

performance for others of the 19 LUCs simulated by the resistance scheme of Zhang *et al.*,[20] in particular, forests.[3]

Conflicts of interest

There are no conflicts to declare.

Acknowledgements

We thank Johannes Fritsche for providing high-resolution Hg^0 flux data from the Swiss grassland site. We also thank the anonymous reviewers for their constructive comments. This research was funded by the U.S. National Science Foundation through Grants #ICER-1313755 (PI: Perlinger), #OPP-1304305; 1739567 (PI: Obrist), and #AGS-1848212 (PI: Obrist).

References

1 W. Zhu, C.-J. Lin, X. Wang, J. Sommar, X. Fu and X. Feng, Global observations and modeling of atmosphere–surface exchange of elemental mercury: a critical review, *Atmos. Chem. Phys.*, 2016, **16**, 4451–4480.

2 C. S. Eckley, M. T. Tate, C.-J. Lin, M. Gustin, S. Dent, C. Eagles-Smith, M. A. Lutz, K. P. Wickland, B. Wang and J. E. Gray, Surface-air mercury fluxes across Western North America: A synthesis of spatial trends and controlling variables, *Sci. Total Environ.*, 2016, **568**, 651–665.

3 Y. Agnan, T. Le Dantec, C. W. Moore, G. C. Edwards and D. Obrist, New constraints on terrestrial surface–atmosphere fluxes of gaseous elemental mercury using a global database, *Environ. Sci. Technol.*, 2016, **50**, 507–524.

4 D. Obrist, J. L. Kirk, L. Zhang, E. M. Sunderland, M. Jiskra and N. E. Selin, A review of global environmental mercury processes in response to human and natural perturbations: Changes of emissions, climate, and land use, *Ambio*, 2018, **47**, 116–140.

5 S. Y. Kwon and N. E. Selin, Uncertainties in atmospheric mercury modeling for policy evaluation, *Curr. Pollut. Rep.*, 2016, **2**, 103–114.

6 M. Jiskra, J. E. Sonke, D. Obrist, J. Bieser, R. Ebinghaus, C. L. Myhre, K. A. Pfaffhuber, I. Wängberg, K. Kyllönen and D. Worthy, A vegetation control on seasonal variations in global atmospheric mercury concentrations, *Nat. Geosci.*, 2018, **11**, 244.

7 J. D. Demers, J. D. Blum and D. R. Zak, Mercury isotopes in a forested ecosystem: Implications for air-surface exchange dynamics and the global mercury cycle, *Global Biogeochem. Cycles*, 2013, **27**, 222–238.

8 M. Jiskra, J. G. Wiederhold, U. Skyllberg, R.-M. Kronberg, I. Hajdas and R. Kretzschmar, Mercury deposition and re-emission pathways in boreal forest soils investigated with Hg isotope signatures, *Environ. Sci. Technol.*, 2015, **49**, 7188–7196.

9 W. Zheng, D. Obrist, D. Weis and B. A. Bergquist, Mercury isotope compositions across North American forests, *Global Biogeochem. Cycles*, 2016, **30**, 1475–1492.

10 M. Enrico, G. l. L. Roux, N. Marusczak, L.-E. Heimbürger, A. Claustres, X. Fu, R. Sun and J. E. Sonke, Atmospheric mercury transfer to peat bogs dominated by gaseous elemental mercury dry deposition, *Environ. Sci. Technol.*, 2016, **50**, 2405–2412.

11 X. Wang, J. Luo, R. Yin, W. Yuan, C.-J. Lin, J. Sommar, X. Feng, H. Wang and C. Lin, Using mercury isotopes to understand mercury accumulation in the montane forest floor of the Eastern Tibetan Plateau, *Environ. Sci. Technol.*, 2016, **51**, 801–809.

12 D. Obrist, Y. Agnan, M. Jiskra, C. L. Olson, D. P. Colegrove, J. Hueber, C. W. Moore, J. E. Sonke and D. Helmig, Tundra uptake of atmospheric elemental mercury drives Arctic mercury pollution, *Nature*, 2017, **547**, 201.

13 M. S. Gustin, S. E. Lindberg and P. J. Weisberg, An update on the natural sources and sinks of atmospheric mercury, *Appl. Geochem.*, 2008, **23**, 482–493.

14 E. S. Corbitt, D. J. Jacob, C. D. Holmes, D. G. Streets and E. M. Sunderland, Global source–receptor relationships for mercury deposition under present-day and 2050 emissions scenarios, *Environ. Sci. Technol.*, 2011, **45**, 10477–10484.

15 H. M. Amos, D. J. Jacob, D. G. Streets and E. M. Sunderland, Legacy impacts of all-time anthropogenic emissions on the global mercury cycle, *Global Biogeochem. Cycles*, 2013, **27**, 410–421.

16 J. S. Hartman, P. J. Weisberg, R. Pillai, J. A. Ericksen, T. Kuiken, S. E. Lindberg, H. Zhang, J. J. Rytuba and M. S. Gustin, Application of a rule-based model to estimate mercury exchange for three background biomes in the continental United States, *Environ. Sci. Technol.*, 2009, **43**, 4989–4994.

17 M. Wesely, Parameterization of surface resistances to gaseous dry deposition in regional-scale numerical models, *Atmos. Environ.*, 1989, **23**, 1293–1304.

18 J. L. Walmsley and M. L. Wesely, Modification of coded parametrizations of surface resistances to gaseous dry deposition, *Atmos. Environ.*, 1996, **30**, 1181–1188.

19 M. Wesely and B. Hicks, A review of the current status of knowledge on dry deposition, *Atmos. Environ.*, 2000, **34**, 2261–2282.

20 L. Zhang, J. Brook and R. Vet, A revised parameterization for gaseous dry deposition in air-quality models, *Atmos. Chem. Phys.*, 2003, **3**, 2067–2082.

21 P. Pai, P. Karamchandani and C. Seifneur, Simulation of the regional atmospheric transport and fate of mercury using a comprehensive Eulerian model, *Atmos. Environ.*, 1997, **31**, 2717–2732.

22 A. P. Dastoor and Y. Larocque, Global circulation of atmospheric mercury: a modelling study, *Atmos. Environ.*, 2004, **38**, 147–161.

23 N. E. Selin, D. J. Jacob, R. M. Yantosca, S. Strode, L. Jaeglé and E. M. Sunderland, Global 3-D land-ocean-atmosphere model for mercury: Present-day *versus* preindustrial cycles and anthropogenic enrichment factors for deposition, *Global Biogeochem. Cycles*, 2008, **22**(2), DOI: 10.1029/2007GB003040.

24 S. Song, N. E. Selin, A. L. Soerensen, H. Angot, R. Artz, S. Brooks, E.-G. Brunke, G. Conley, A. Dommergue and R. Ebinghaus, Top-down constraints on atmospheric mercury emissions and implications for global biogeochemical cycling, *Atmos. Chem. Phys.*, 2015, **15**, 7103–7125.

25 G. Jung, I. Hedgecock and N. Pirrone, ECHMERIT V1. 0–a new global fully coupled mercury-chemistry and transport model, *Geosci. Model Dev.*, 2009, **2**, 175–195.

26 D. Durnford, A. Dastoor, A. Ryzhkov, L. Poissant, M. Pilote and D. Figueras-Nieto, How relevant is the deposition of mercury onto snowpacks?–Part 2: A modeling study, *Atmos. Chem. Phys.*, 2012, **12**, 9251–9274.

27 O. Travnikov, J. Jonson, A. Andersen, M. Gauss, A. Gusev, O. Rozovskaya, D. Simpson, V. Sokovyh, S. Valiyaveetil and P. Wind, *Development of the EMEP global modelling framework: Progress report*, EMEP/MSC-E Technical Report 7/2009, Meteorological Synthesizing Centre-East of EMEP, Moscow, 2009.

28 I. Consulting, *User's Guide to the Regional Modeling System for Aerosols and Deposition (REMSAD)*, Version 7, 2002.

29 H. Lei, X.-Z. Liang, D. J. Wuebbles and Z. Tao, Model analyses of atmospheric mercury: present air quality and effects of transpacific transport on the United States, *Atmos. Chem. Phys.*, 2013, **13**, 10807–10825.

30 C. N. Gencarelli, J. Bieser, F. Carbone, F. De Simone, I. M. Hedgecock, V. Matthias, O. Travnikov, X. Yang and N. Pirrone, Sensitivity model study of regional mercury dispersion in the atmosphere, *Atmos. Chem. Phys.*, 2017, **17**, 627–643.

31 J. O. Bash, Description and initial simulation of a dynamic bidirectional air-surface exchange model for mercury in Community Multiscale Air Quality (CMAQ) model, *J. Geophys. Res.: Atmos.*, 2010, **115**(D6), DOI: 10.1029/2009JD012834.

32 Z. Wu, X. Wang, F. Chen, A. A. Turnipseed, A. B. Guenther, D. Niyogi, U. Charusombat, B. Xia, J. W. Munger and K. Alapaty, Evaluating the calculated dry deposition velocities of reactive nitrogen oxides and ozone from two community models over a temperate deciduous forest, *Atmos. Environ.*, 2011, **45**, 2663–2674.

33 B. B. Hicks, R. D. Saylor and B. D. Baker, Dry deposition of particles to canopies—A look back and the road forward, *J. Geophys. Res.: Atmos.*, 2016, **121**, 14691–14707.

34 C. Flechard, E. Nemitz, R. Smith, D. Fowler, A. Vermeulen, A. Bleeker, J. Erisman, D. Simpson, L. Zhang and Y. Tang, Dry deposition of reactive nitrogen to European ecosystems: a comparison of inferential models across the NitroEurope network, *Atmos. Chem. Phys.*, 2011, **11**, 2703–2728.

35 Z. Wu, D. B. Schwede, R. Vet, J. T. Walker, M. Shaw, R. Staebler and L. Zhang, Evaluation and intercomparison of five North American dry deposition algorithms at a mixed forest site, *J. Adv. Model. Earth Syst.*, 2018, **10**, 1571–1586.

36 L. Zhang, L. P. Wright and P. Blanchard, A review of current knowledge concerning dry deposition of atmospheric mercury, *Atmos. Environ.*, 2009, **43**, 5853–5864.

37 L. Poissant and A. Casimir, Water-air and soil-air exchange rate of total gaseous mercury measured at background sites, *Atmos. Environ.*, 1998, **32**, 883–893.

38 X. Xu, X. Yang, D. R. Miller, J. J. Helble and R. J. Carley, Formulation of bi-directional atmosphere-surface exchanges of elemental mercury, *Atmos. Environ.*, 1999, **33**, 4345–4355.

39 H. Zhang, S. E. Lindberg, F. Marsik and G. J. Keeler, Mercury air/surface exchange kinetics of background soils of the Tahquamenon River watershed in the Michigan Upper Peninsula, *Water, Air, Soil Pollut.*, 2001, **126**, 151–169.

40 X. Lin and Y. Tao, A numerical modelling study on regional mercury budget for eastern North America, *Atmos. Chem. Phys.*, 2003, **3**, 535–548.

41 J. O. Bash, D. R. Miller, T. H. Meyer and P. A. Bresnahan, Northeast United States and Southeast Canada natural mercury emissions estimated with a surface emission model, *Atmos. Environ.*, 2004, **38**, 5683–5692.

42 P. K. Gbor, D. Wen, F. Meng, F. Yang, B. Zhang and J. J. Sloan, Improved model for mercury emission, transport and deposition, *Atmos. Environ.*, 2006, **40**, 973–983.

43 C.-J. Lin, M. S. Gustin, P. Singhasuk, C. Eckley and M. Miller, Empirical models for estimating mercury flux from soils, *Environ. Sci. Technol.*, 2010, **44**, 8522–8528.

44 N. V. Smith-Downey, E. M. Sunderland and D. J. Jacob, Anthropogenic impacts on global storage and emissions of mercury from terrestrial soils: Insights from a new global model, *J. Geophys. Res.: Biogeosci.*, 2010, **115**(G3), DOI: 10.1029/2009JG001124.

45 N. Pirrone, W. Aas, S. Cinnirella, R. Ebinghaus, I. M. Hedgecock, J. Pacyna, F. Sprovieri and E. M. Sunderland, Toward the next generation of air quality monitoring: Mercury, *Atmos. Environ.*, 2013, **80**, 599–611.

46 X. Wang, C. J. Lin and X. Feng, Sensitivity analysis of an updated bidirectional air–surface exchange model for elemental mercury vapor, *Atmos. Chem. Phys.*, 2014, **14**, 6273–6287.

47 L. P. Wright and L. Zhang, An approach estimating bidirectional air-surface exchange for gaseous elemental mercury at AMNet sites, *J. Adv. Model. Earth Syst.*, 2015, **7**, 35–49.

48 W. Yuan, J. Sommar, C.-J. Lin, X. Wang, K. Li, Y. Liu, H. Zhang, Z. Lu, C. Wu and X. Feng, Stable isotope evidence shows re-emission of elemental mercury vapor occurring after reductive loss from foliage, *Environ. Sci. Technol.*, 2018, **53**, 651–660.

49 J. Fritsche, D. Obrist, M. J. Zeeman, F. Conen, W. Eugster and C. Alewell, Elemental mercury fluxes over a sub-alpine grassland determined with two micrometeorological methods, *Atmos. Environ.*, 2008, **42**, 2922–2933.

50 C. L. Olson, M. Jiskra, J. E. Sonke and D. Obrist, Mercury in tundra vegetation of Alaska: Spatial and temporal dynamics and stable isotope patterns, *Sci. Total Environ.*, 2019, **660**, 1502–1512.

51 J. E. Hobbie and G. W. Kling, *Alaska's changing Arctic: Ecological consequences for tundra, streams, and lakes*, Oxford University Press, 2014.

52 C. Olson, M. Jiskra, H. Biester, J. Chow and D. Obrist, Mercury in Active-Layer Tundra Soils of Alaska: Concentrations, Pools, Origins, and Spatial Distribution, *Global Biogeochem. Cycles*, 2018, **32**, 1058–1073.

53 O. DAAC, *MODIS Collection 6 Land Products Global Subsetting and Visualization Tool*, accessed March 28, 2017.

54 A. Carpi and S. E. Lindberg, Application of a Teflon™ dynamic flux chamber for quantifying soil mercury flux: tests and results over background soil, *Atmos. Environ.*, 1998, **32**, 873–882.

55 C. Moore and A. Carpi, Mechanisms of the emission of mercury from soil: Role of UV radiation, *J. Geophys. Res.*, 2005, **110**(D24), DOI: 10.1029/2004JD005567.

56 D. L. Liu, Incorporating diurnal light variation and canopy light attenuation into analytical equations for calculating daily gross photosynthesis, *Ecol. Modell.*, 1996, **93**, 175–189.

57 D. Kocman and M. Horvat, Non-point source mercury emission from the Idrija Hg-mine region: GIS mercury emission model, *J. Environ. Manage.*, 2011, **92**, 2038–2046.

58 D. Obrist, A. K. Pokharel and C. Moore, Vertical profile measurements of soil air suggest immobilization of gaseous elemental mercury in mineral soil, *Environ. Sci. Technol.*, 2014, **48**, 2242–2252.

59 A. Rea, S. Lindberg, T. Scherbatskoy and G. J. Keeler, Mercury accumulation in foliage over time in two northern mixed-hardwood forests, *Water, Air, Soil Pollut.*, 2002, **133**, 49–67.

60 A. P. Rutter, J. J. Schauer, M. M. Shafer, J. Creswell, M. R. Olson, A. Clary, M. Robinson, A. M. Parman and T. L. Katzman, Climate sensitivity of gaseous elemental mercury dry deposition to plants: impacts of temperature, light intensity, and plant species, *Environ. Sci. Technol.*, 2010, **45**, 569–575.

61 M. R. Risch, J. F. DeWild, D. A. Gay, L. Zhang, E. W. Boyer and D. P. Krabbenhoft, Atmospheric mercury deposition to forests in the eastern USA, *Environ. Pollut.*, 2017, **228**, 8–18.

62 J. T. Arredondo and H. Schnyder, Components of leaf elongation rate and their relationship to specific leaf area in contrasting grasses, *New Phytol.*, 2003, **158**, 305–314.

63 X. Wang, Z. Bao, C.-J. Lin, W. Yuan and X. Feng, Assessment of global mercury deposition through litterfall, *Environ. Sci. Technol.*, 2016, **50**, 8548–8557.

64 C. L. Olson, M. Jiskra, J. E. Sonke and D. Obrist, Mercury in tundra vegetation of Alaska: Spatial and temporal dynamics and stable isotope patterns, *Sci. Total Environ.*, 2019, **660**, 1502–1512.

65 J. A. Foley, R. DeFries, G. P. Asner, C. Barford, G. Bonan, S. R. Carpenter, F. S. Chapin, M. T. Coe, G. C. Daily and H. K. Gibbs, Global consequences of land use, *Science*, 2005, **309**, 570–574.

66 C. M. Iversen, V. L. Sloan, P. F. Sullivan, E. S. Euskirchen, A. D. McGuire, R. J. Norby, A. P. Walker, J. M. Warren and S. D. Wullschleger, The unseen iceberg: plant roots in arctic tundra, *New Phytol.*, 2015, **205**, 34–58.

67 S. J. Silva and C. L. Heald, Investigating dry deposition of ozone to vegetation, *J. Geophys. Res.: Atmos.*, 2018, **123**, 559–573.

